Am J Transl Res 2020;12(11):7079-7095
www.ajtr.org /ISSN:1943-8141/AJTR0117777

Original Article

Nano-biological mesh constructed by astragaloside-IV-induced bone marrow mesenchymal stem cells on PLGA-NPs-SIS can be used for abdominal wall reconstruction

Xiaowen Li*, Da Lin*, Yaqian Chen*, Haimin Jin, Zhongkai Ni, Hai Huang

*Department of General Surgery, Guangxing Affiliated Hospital of Zhejiang Chinese Medical University, Hangzhou 310007, Zhejiang Provincial, China. *Equal contributors and co-first authors.*

Received July 8, 2020; Accepted October 11, 2020; Epub November 15, 2020; Published November 30, 2020

Abstract: A combination of stem cells, scaffold materials, nanoparticles (NPs), and physiological factors can be used to engineer a tissue that can replace or improve the function of the damaged tissue. This study was designed to assess whether astragaloside (aS)-IV-activated rat bonemarrow-derived mesenchymal stem cells (BMSCs), seeded on a nano-biological mesh composed of small intestinal submucosa (SIS) modified with poly (D,L-lactide-co-glycolide) NPs (PLGA-NPs-SIS), can promote cell engraftment, proliferation, and mesh incorporation into the tissue upon implantation. aS-IV-induced BMSCs cultured with PLGA-NPs-SIS showed enhanced viability and proliferation as well as reduced apoptosis. Vascular endothelial growth factor, type I and II collagen, and monocyte chemoattractant protein-1 were upregulated, whereas matrix metalloproteinase and interleukin-6 were downregulated in these BMSCs. Pre-seeded BMSCs induced with aS-IV engrafted in a rat abdominal wall defect model showed migratory and proliferative capacities while enhancing vascularity at the musculofascial/graft interface. These findings imply that the nano-biological mesh composed of aS-IV-induced BMSCs seeded on PLGA-NPs-SIS can be used for abdominal wall reconstruction.

Keywords: Astragaloside IV, bone marrow-derived mesenchymal stem cell, poly (D,L-lactide-co-glycolide) nanoparticle, abdominal wall reconstruction, tissue engineerin

Introduction

The most common abdominal wall defects include inguinal and ventral hernias, which are complications of abdominal laparotomy. Approximate 10% of the population suffers from some type of abdominal wall hernia in their lifetime [1]; as such, abdominal wall reconstruction is one of the most common operations performed by general surgeons. However, there is no single approach that is universally effective, and complications such as infection and recurrence are still a clinical challenge.

Synthetic scaffolds including polypropylene and expanded polytetrafluoroethylene are usually used for abdominal wall reconstruction [2, 3]. However, an implanted foreign body can elicit a chronic inflammatory reaction and is not under remodeling by the host [4]. Synthetic meshes are also associated with increased risks of infection, adhesion to the bowels, and enterocutaneous fistula formation. Biological scaffolds composed of extracellular matrix (ECM) components from human and animal tissues, such as the dermis, pericardium, as well as small intestine submucosa (SIS) [5, 6], are a promising alternative to synthetic materials.

SIS from porcine small intestine has been extensively investigated for its ability of repairing abdominal wall defects [7-9]. Multilaminated SIS provides mechanical strength for tissue regeneration but also promotes cellular infiltration and vascularization [10]. In addition, SIS is resistant to bacterial infection even in contaminated surgical fields, tolerates exposure without requiring explanation; resists adhesion, and

strengthens the musculofascial interface in the early stages of tissue repair [11].

One limitation of SIS is the microarchitectural heterogeneity that can lead to inconsistent results. Previous studies reported that bone marrow mesenchymal stem cells (BMSCs) on an SIS scaffold accelerate re-epithelialization, revascularization, as well as muscle regeneration in the esophagus [12]; in addition, SIS supports the 3D growth of BMSCs *in vitro*, and BMSC-seeded SIS scaffolds promote the regeneration of bladder in a canine model [13]. Thus, BMSCs can be as adopted as a cell source in tissue engineering.

Astragaloside (aS)-IV, a constituent of the root extract of *Astragalus* species, is widely used in Chinese traditional medicine and shows good biocompatibility [14]. MSCs treated with tanshinone IIA and aS-IV express a higher C-X-C chemokine receptor type 4 level on the cell surface compared with untreated control cells [15]. Additionally, aS-IV treatment promotes the expression of the stem cell factor, granulocyte macrophage colony stimulating factor, thrombopoietin, as well as transforming growth factor (TGF)-β1 in MSCs [16].

Poly (D,L-lactide-co-glycolide) (PLGA) is a biodegradable and biocompatible copolymer that has been authorized by the U.S. Food and Drug Administration for clinical use (e.g., in therapeutic devices) [17]. PLGA/collagen (COL)I microspheres combined with BMSCs have been used for trabecular reconstruction, and improve bone quality in osteoporotic rats [18]. Moreover, abdominal defects were successfully repaired using polyglycolic acid fibers and the corresponding cell type in an animal model, preventing postoperative peritoneal adhesion [19].

Based on the above, we hypothesized that proliferating stem cells in SIS would enhance cellular and vascular infiltration from surrounding tissues. Therefore, this study aimed to assess whether BMSCs induced by astragaloside IV and integrated into SIS modified by PLGA nanoparticles (NPs) can promote stem cell engraftment, survival, and proliferation. Our findings indicate that the nano-biological mesh composed of aS-IV-induced BMSCs seeded on PLGA-NPs-SIS is effective for abdominal wall reconstruction.

Methods and materials

Moral statement

This study was approved by the Ethics Committee of our hospital. The animal experiment was also approved by the Institutional Animal Care and Use Committee of our hospital, and the operation process was carried out in strict accordance with the relevant guidelines.

Preparation and detection of PLGA NPs

PLGA (0.4 g) was soaked in 15 ml solution supplemented with acetone and chloroform (9:6, v/v) under a fume hood. The solution was combined with 40 ml deionized water through stirring at 400 rpm for 30 min. Solvent evaporation was carried out using a rotary evaporator. After centrifugation at 12,000 rpm, PLGA in the emulsion was detected on a laser particle size analyzer and characterized through transmission electron microscopy (TEM). The concentration of the nanoscale solution was determined by the dry weight method [20].

Preparation of SIS

Porcine small intestine was acquired from healthy pigs within 4 h of killing them and cut into pieces of about 10 cm in length, which were washed with normal saline. The tunica serosa and muscularis were manually taken out to obtain the SIS, which was washed with normal saline and soaked in a solution with methanol and chloroform (1:1, v/v) under a fume hood for 12 h. After three washes through deionized water to remove organic solvents, the sample was subjected to 12-h incubation with 0.05% trypsin/0.05% ethylenediaminetetraacetic acid (EDTA) at 37°C, washed with normal saline to remove trypsin, and processed by 0.5% sodium dodecyl sulfate for 4 h with periodic vortexing. After washing with normal saline, the sample was soaked in 0.1% peroxyacetic acid + 20% ethanol for 30 minutes, washed with normal saline, and dried in a freeze dryer.

BMSCs

Adult male rats were euthanized via CO_2 inhalation, and the femur and tibia were dissected and placed in pre-cooling Dulbecco's modified

Eagle's medium (DMEM). The epiphyses of the femur and tibia were removed, and the bone marrow was washed off through a syringe filled with DMEM. The bone marrow was gently aspirated and triturated to obtain a single-cell suspension that was subjected to 1000 rpm centrifugation for 20 min. The cell pellet was resuspended in complete medium in a culture flask. About 72 h after plating, the culture supernatant with non-adherent cells was taken out, and fresh medium was added. At 80% confluence, cells were passaged two to five times by digestion through 0.25% trypsin in 1 mM EDTA for 5 min and subcultured at 1:2.

Physical properties of PLGA NP-modified SIS

SIS was transferred to wells constructed with silicone glue on the mucosal side, and PLGA NP suspensions at 1.273 mg/cm^2 were added into the mucosal side of SIS. The assembly was incubated overnight on a shaker at 37°C. The NP-modified SIS membrane was washed with water to remove unattached NPs, and thickness was measured as previously described [21]. Briefly, the membrane was cut into small (2 × 10 mm) sections, and digital micrographs of the cross section were acquired under an inverted microscope accompanied by a charge-coupled device camera. The cross-sectional distance was metered with the Sigma Scan Pro (Systat, Point Richmond, CA, USA) calibrated through an image of a hemocytometer. Briefly, analysis on 6 × 1-cm strips of NP-modified SIS membrane were carried out through an electromechanical load frame (Model 5842; Instron, Canton, MA, USA) with a constant crosshead velocity (10 mm/min). Tests were carried out under dehydration at 37°C in a custom-made chamber.

Cell proliferation assay

The proliferation of transplanted BMSCs was evaluated based on bromodeoxyuridine (BrdU) incorporation. When BMSCs reached the logarithmic growth phase, BrdU was added into the culture at 30 μM. After 30-60 min, cells were harvested by 1000 × *g* centrifugation for 10 min. After two rinses through 500 μl wash buffer, 10^5-10^6 cells were transferred to a tube, and 500 μl fixation buffer was added, followed by overnight incubation at 4°C. The cells were cleaned twice with 500 μl wash buffer for 2 min at 4°C, and 300 μl denaturation buffer was added at 37°C for 30 min, followed by two rinses and the addition of 195 μl dye buffer and 5 μl fluorescein isothiocyanate (FITC)-BrdU. Labeled cells were determined via flow cytometry at excitation and emission wavelengths of 488 and 520 nm, respectively.

Cell viability assay

A Cell Counting Kit (CCK)-8 kit was adopted for detection of viable cells. Briefly, 100 μl cell suspensions (5 × 10^4/ml) were transferred to 96-well plates, followed by 24-h incubation in a 5% CO_2 incubator at 37°C. After two washes, 200 μl serum-free α-minimal essential medium was added for 24 h. CCK-8 solution (10-μl in volume) was added for 3 h, and cell viability was determined by metering the absorbance at 450 nm on a microplate reader.

Detection of apoptotic BMSCs by annexin-V FITC/propidium iodide (PI) double staining

Annexin-V FITC/PI double staining was carried out to detect apoptotic BMSCs *in vitro*. Cells grown for 24 h were collected and washed three times. After being added with 500 μl binding buffer, 5 μl Annexin V-FITC, and 5 μl PI, the cells were subjected to 15-min incubation at room temperature.

Apoptotic cells were determined via flow cytometry at excitation and emission wavelengths of 488 and 530 nm, respectively.

Immunofluorescence

To evaluate collagen secretion by BMSCs, the cells were immobilized by 4% paraformaldehyde for 30 min, rinsed three times with phosphate-buffered saline (PBS), and treated by 3% H_2O_2-methanol to inactivate endogenous peroxidase. The samples were immersed in 50 μl normal goat serum for 20 min and cultured with antibodies targeting pro-COLI/III (1:200) for 2 h. After washing with PBS, the specimens were cultured for 1 h at 37°C with FITC/tetramethylrhodamine-conjugated secondary antibodies (1:200), washed three times, and stained with 50 μl 4',6-diamidino-2-phenylindole (DAPI) for 5 min. Immunoreactive cells were counted under an inverted epifluorescence microscope (IX51; Olympus, Tokyo, Japan).

Rat abdominal wall defect model

Male Sprague-Dawley rats (n = 45, 250 ± 10 g) were anesthetized through intraperitoneal

Table 1. Primer for real-time PCR

Primer	Sequences (5'- > 3')
Collagen I - Forward	CGTGGAAACCTGATGTATGC
Collagen I - Reverse	GGTTGGGACAGTCCAAGTCT
Collagen III - Forward	GATGCTGGTGCTGAGAAGAA
Collagen III - Reverse	GGCTGGAAAGAAGTCTGAGG
IL-6 - Forward	GAGAAAAGAGTTGTGCAATGGC
IL-6 - Reverse	ACTAGGTTTGCCGAGTAGACC
MCP-1 - Forward	ATGCAGGTCTCTGTCACGCT
MCP-1 - Reverse	GGTGCTGAAGTCCTTAGGGT
MMP-9 - Forward	TTCAAGGACGGTCGGTATT
MMP-9 - Reverse	CTCTGAGCCTAGCCCCAACTTA
VEGF - Forward	GCAGCTTGAGTTAAACGAACG
VEGF - Reverse	AGTTCCCGAAACCCTGAG
GADPH - Forward	GGCCTTCCGTGTTCCTACC
GADPH - Reverse	CGCCTGCTTCACCACCTTC

injection of 10% chloral hydrate (4 ml/kg). The fur on the abdomen was shaved and the skin was disinfected. A full-thickness defect (2.0 × 2.0 cm) was caused in the abdominal wall while retaining the abdominal surface of the skin and subcutaneous tissues. No mesh was implanted in the model group, and the skin was sutured by a 3-0 suture. In the test group, a patch was implanted along with the engineered tissue scaffolds with an overlap of about 0.5 cm, and the skin was closed with a 3-0 suture.

Rats were assigned to five groups (n = 8 animals each): group 1, normal; group 2, abdominal wall defect model; group 3, polypropylene patch implantation (PP); group 4, implantation of SIS modified with PLGA NPs seeded with BMSCs (BSP); and group 5, implantation of SIS modified with PLGA NPs seeded with BMSCs induced with astragaloside IV (ABSP). Body weight, eating behavior, infection, hematoma formation, and mortality were monitored throughout the study. At 1, 4, and 8 weeks after implantation, three animals per group were sacrificed to evaluate adhesion and for histological analyses.

Evaluation of adhesion

The adhesion area was determined as a proportion of the total visible implant area on micrographs. Adhesion strength was semi-quantitatively graded on a scale from 0 to 3 in an increment of 0.5 as follows: 0, no adhesion; 1, adhesion easily separated by applying gentle force; 2, adhesion separable by blunt dissection; and 3, adhesion requiring sharp dissection for separation from the implant site.

Hematoxylin-eosin (H&E) and Masson's trichrome staining

Two-cm-long tissue sections were excised from the abdominal wall at 1, 4, and 8 weeks after operation, respectively, and fixed with 10% formalin. After being cut at a thickness of 5 mm, paraffin sections were dyed with H&E and Masson's trichrome, respectively.

Immunohistochemistry

Immunohistochemistry was carried out on paraffin sections sliced at 5-7 μm. The sections were deparaffinized through hot water, rinsed three times through PBS, boiled in citrate buffer, and incubated in 3% H_2O_2-methanol for 10 min for inactivation of endogenous peroxidase. The sections were then successively cultured with goat serum and primary antibodies (1:100) for 2 h at 37°C. Subsequently, 50 μl horseradish peroxidase-conjugated IgG-Fab fragment was added for 2 h at 37°C. After rinse, two drops of diaminobenzidine solution were added, followed by rinsing with distilled water to terminate the chromogenic reaction. The sections were counterstained through H&E, dehydrated, mounted, and evaluated under a light microscope (Nikon, Tokyo, Japan).

Quantitative real-time (qRT)-PCR

Total RNA was extracted with TRIzol reagent (Invitrogen, Carlsbad, CA, USA) under the manufacturer's instructions. First strand cDNA was synthesized with 2 mg total RNA through the Superscript first-strand synthesis system (Invitrogen). The levels of octamer-binding protein-4, matrix metalloproteinase (MMP)-9, (sex determining region Y)-box-2, COLI, COLIII, interleukin (IL)-6, monocyte chemotactic protein (MCP)-1, as well as vascular endothelial growth factor (VEGF) were determined via qRT-PCR on an ABI Step One Plus Real time-PCR system (Applied Biosystems, Foster City, CA, USA). Glyceraldehyde 3-phosphate dehydrogenase (GAPDH) was adopted for normalization. Primer sequences are listed as **Table 1**. The cycling conditions: 95°C for 5 min; 42 cycles of 95°C for 15 s and 60°C for 20 s; and 72°C for 40 s.

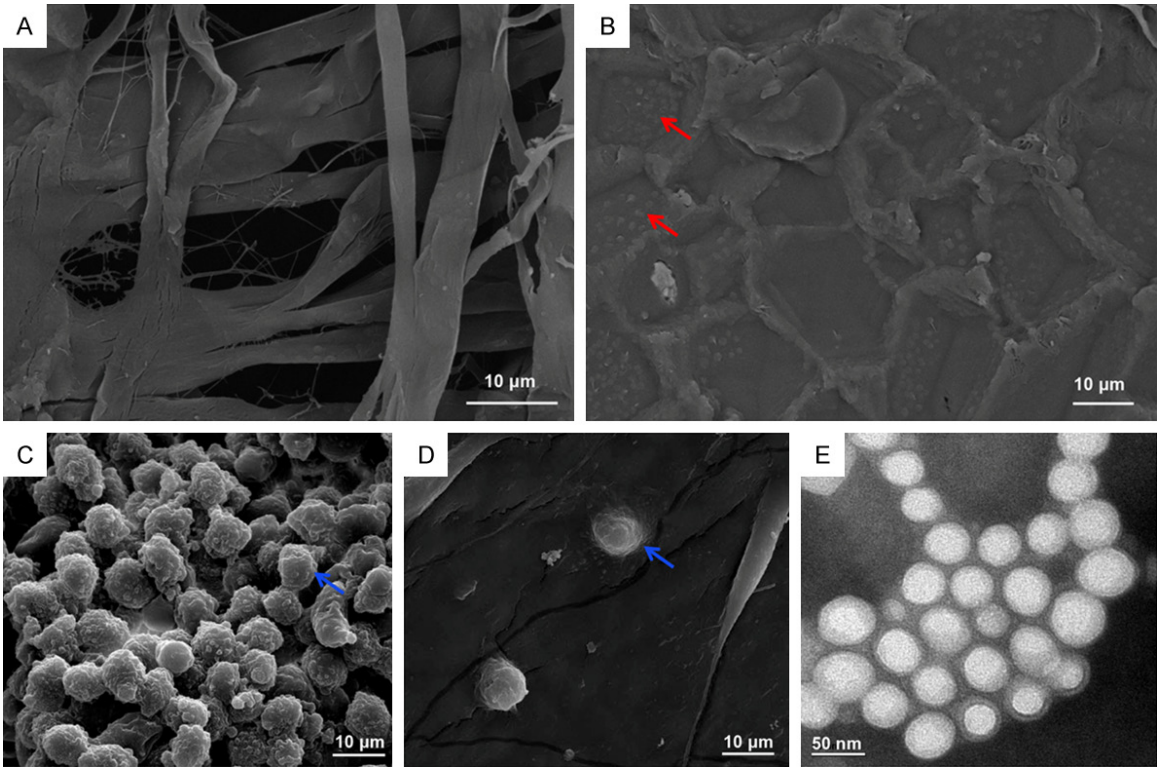

Figure 1. Characteristics of the nano-biological mesh. SEM images of SIS close to the serosal layer (A), SIS close to the mucosal layer (B), BMSC-SIS-PLGA mesh close to the serosal layer (C), and BMSC-SIS-PLGA mesh close the mucosal layer (D). TEM image of PLGA NPs (E). Red and blue arrows indicate PLGA NPs and BMSCs, respectively. Scale bar = 10 μm in (A-D). Scale bar = 50 nm in (E).

Western blotting (WB)

Proteins were extracted from tissue by radioimmunoprecipitation assay (RIPA) buffer, and total protein amounts were detected by the bicinchoninic acid assay. Proteins were isolated through polyacrylamide gel electrophoresis with a 12% separation gel and 5% stacking gel, and transferred to a membrane, and the membrane was then immersed in 5% nonfat dry milk in PBS for 2 h at indoor temperature. After three washes through Tris-buffered saline containing 0.1% Tween-20 (TBST), the membrane was cultured with primary antibodies at 4°C all night long. After three washes through TBST, 10 min each time, the membrane was cultured through fluorophore-conjugated secondary antibodies for 1 h at indoor temperature. Protein bands were evaluated on an Odyssey imaging system (LI-COR, Lincoln, NE, USA).

Statistical analyses

Experiments were repeated three times at least. Data are expressed as the mean ± standard deviation (SD), compared among multiple groups using the One-way analysis of variance (ANOVA); inter-group differences were evaluated through the Student's t-test. SPSS (SPSS Inc., USA) and GraphPad Prism 6 (GraphPad Software Inc., USA) were adopted for data analysis. $P < 0.05$ implies a significant difference.

Results

Characterization of PLGA and BMC-SIS

SIS isolated from pig small intestinal tissues by enzymatic digestion showed fibroblast-like morphology by scanning electron microscope (SEM) analysis as well as good proliferative capacity (**Figure 1A**, **1B**). BMSCs seeded on SIS scaffolds formed a membrane after 5 days of culture (**Figure 1C**, **1D**). Next, PLGA NPs were examined by transmission electron microscope (TEM). The uniform spheres had an average size of 167 nm (**Figure 1E**). The size distribution was determined by analyzing approximately 100 NPs, and the zeta potential was calculated from three samples. The zeta potential of the produced PLGA NPs was 7.1 ± 1.2 mV (mean ±

standard deviation), indicating that they were stable.

Viability of BMSCs on scaffolds

aS-IV stimulated BMSC proliferation in a concentration-dependent manner with the highest rate observed at a concentration of 160 μg/ml (19.83%), as determined by BrdU incorporation (**Figure 2A**). aS-IV-SIS-PLGA had the most potent effect on cell proliferation (26.58%). In addition, CCK-8 assay results showed that the proliferation ability of cells treated with 160 μM aS-IV was significantly improved, and aS-IV-SIS-PLGA cells showed the strongest proliferation activity (**Figure 2B**). These results indicated that PLGA and aS-IV promoted the growth of BMSCs. Consistent with these observations, annexin-V FITC/PI double staining and flow cytometry analysis showed that BMSCs induced with aS-IV at 80 ($P < 0.05$) and 160 ($P > 0.05$) μg/ml before seeding on the SIS-PLGA scaffold suppressed apoptosis compared with normal BMSCs and SIS-PLGA scaffolds seeded with cells not treated with aS-IV (**Figure 2C**).

COLI and COLIII protein quantified by immunofluorescence

BMSCs synthesize collagen, with the most abundant types I and III. The precursor proteins, pro-collagen type I, as well as pro-collagen type III were abundant in the nucleus of BMSCs, as determined by immunocytochemistry (**Figure 3**).

Evaluation of abdominal wall repair following scaffold implantation

All rats that underwent surgery recovered without complications and survived until the end of the study. There was no bleeding, herniation, or wound infection in any of the animals. However, rats with an implanted scaffold showed weight loss and were sluggish.

After implantation of PP, BSP, or ABSP meshes, adhesion areas and strengths were evaluated (**Table 2**). All rats showed slight adhesion involving the omentum. However, in the abdominal wall defect model, adhesion was extensive and affected several additional tissues, including the liver and bowel. Over time, adhesion areas and strengths increased in the model and PP groups, while the opposite trend was observed in the BSP and ABSP groups at 1, 4, and 8 weeks ($P < 0.05$). No significant differences was found between the model and PP groups in adhesion score, whereas at 8 weeks, the ABSP group had a significantly lower adhesion score compared with other groups.

Histological analysis following mesh implantation

In vivo host cell infiltration and inflammatory response to mesh implantation were analyzed at 1, 4, and 8 weeks after operation by examining the structures of the implanted scaffold and the newly formed tissue by H&E staining (**Figure 4**). Multinuclear giant cells were stained with Toluidine Blue. The highest inflammatory response in all experimental groups was found during the first week after operation, but the number of infiltrated inflammatory cells declined over time. Compared with the model group, rats with implants had fewer inflammatory cells, with the lowest number observed in the ABSP group (**Figure 4**).

Collagen is the main component of ECM responsible for tissue repair; its deposition in wound gaps can promote wound contraction and healing. To assess collagen deposition, rats were sacrificed at 1, 4, and 8 weeks, respectively, and the structures of the implanted scaffold and the newly formed tissue-including the distribution and degradation of collagen fibers-were explored by Masson's trichrome staining. Collagen deposition and muscle infiltration increased in area immediately surrounding the graft in the BSP and ABSP groups. At 4 weeks after surgery, the tissue layers in the BSP and ABSP groups were densely aggregated with cells that appeared red after Masson's trichrome staining; these areas reflected newly migrated cells that start to infiltrate the ECM. Most of the collagen fibers were still present 8 weeks after implantation (**Figure 5**). The model group had the lowest abundance of collagen, with the ABSP group showing comparable levels.

Ultrastructure of the abdominal wall tissue assessed by SEM

One specimen at each time point was randomly selected for SEM analysis. Irregular collagen fibrils were observed at 1 week, becoming thicker and more uniform at 4 and 8 weeks

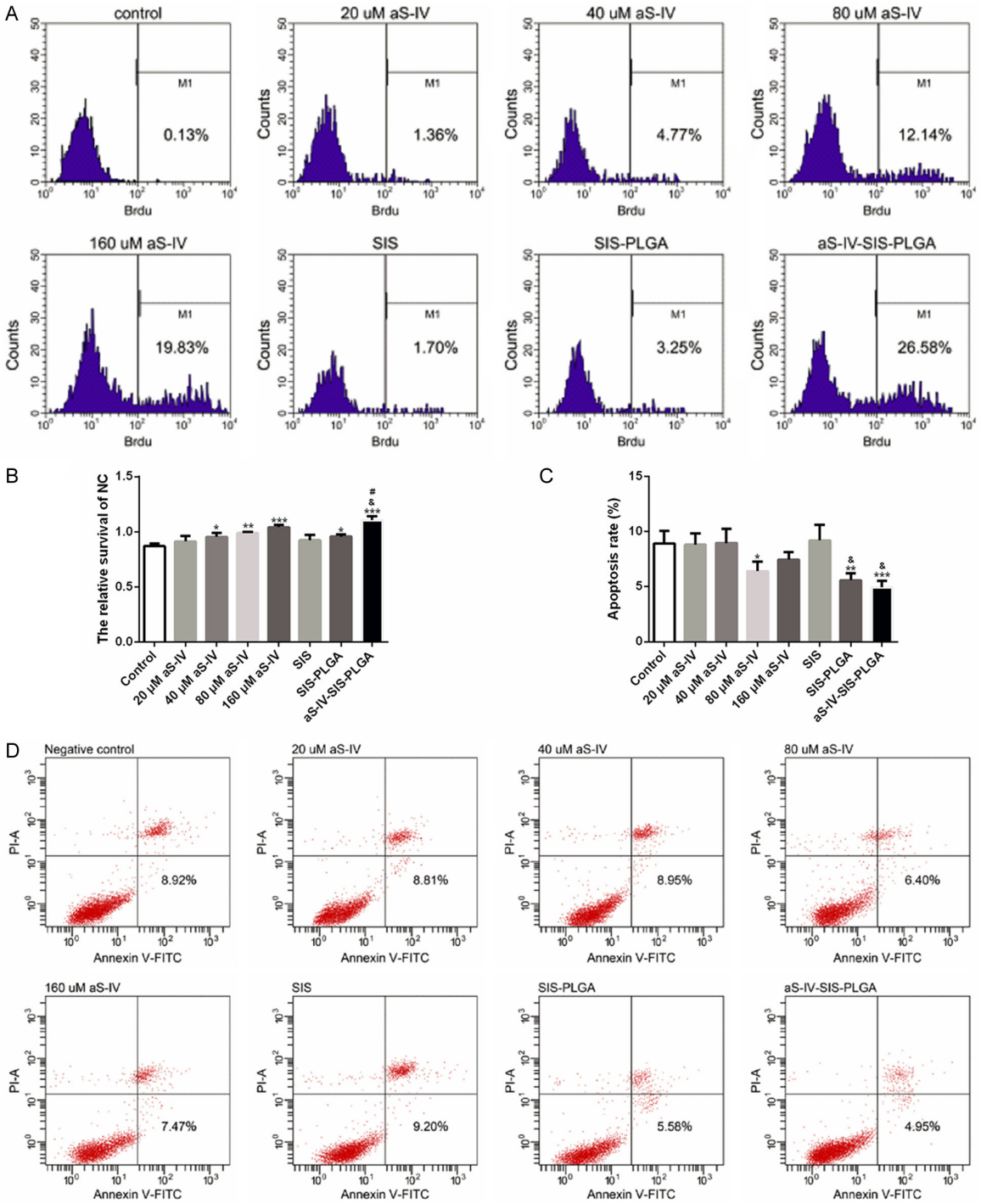

Figure 2. Viability of BMSCs on SIS-PLGA scaffolds. A. Proliferation of BMSCs treated with indicated concentrations of aS-IV. Cell viability in the SIS and SIS-PLGA groups cultured with or without 160 μM aS-IV-induced BMSCs was evaluated by the BrdU incorporation assay. B. Proliferation of BMSCs, as determined by CCK-8. C, D. Apoptosis of BMSCs in the 20-160 μM aS-IV, SIS, and SIS-PLGA groups, and in 160 μM aS-IV-induced BMSCs seeded on SIS-PLGA, as detected via Annexin-V FITC/PI double staining and flow cytometry. *P < 0.05, **P < 0.01, ***P < 0.001, *vs.* control group; $^{\&}$P < 0.05 *vs.* SIS group; $^{\#}$P < 0.05, SIS-PLGA.

(**Figure 6**). The normal group had the thickest and most uniform collagen fibrils, followed by the ABSP, BSP, PP, and model groups in that order.

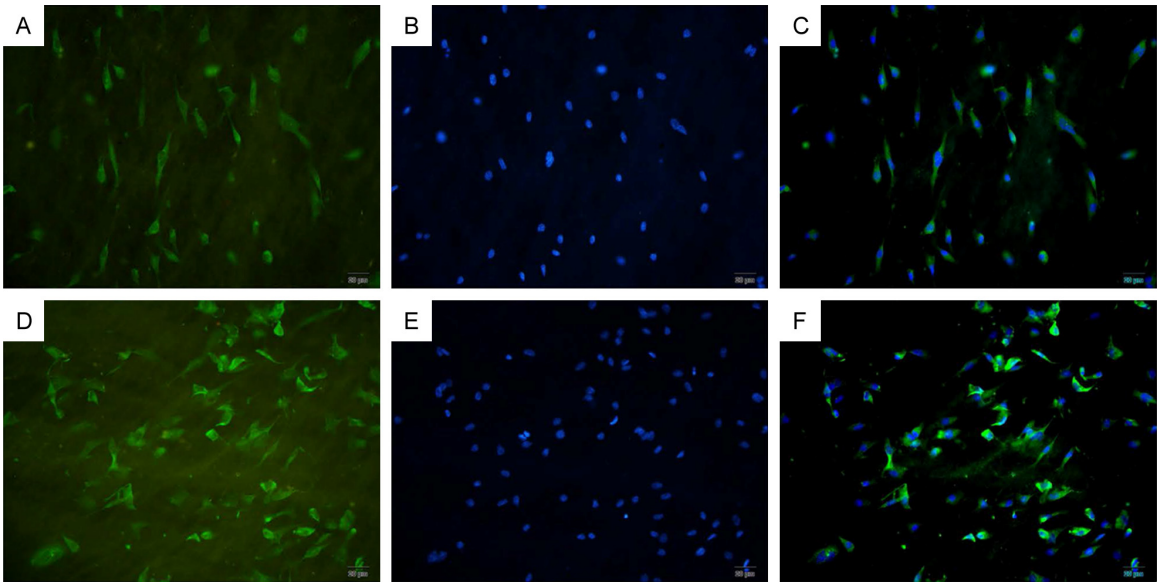

Figure 3. Immunofluorescent detection of COLI and COLIII. COLI (A-C) and COLIII (D-F) expression in BMSCs was detected by immunofluorescence (green). Cells were counterstained through 4',6-diamidino-2-phenylindole (blue).

Table 2. Adhesion areas and scores (mean ± SD) of implanted meshes

	Model group	PP group	BSP group	ABSP group	*P* value
Adhesion areas					
1 week	52.74 ± 2.37$^{*,\dagger,\#}$	29.39 ± 3.31*,†	9.11 ± 0.88	6.58 ± 0.54	< 0.001
4 weeks	79.04 ± 4.56$^{*,\dagger,\#}$	65.09 ± 3.69*,†	8.01 ± 1.45	5.68 ± 0.65	< 0.001
8 weeks	93.20 ± 3.25$^{*,\dagger,\#}$	77.21 ± 3.39*,†	5.82 ± 1.09	3.68 ± 0.46	< 0.001
Adhesion scores					
1 week	2.60 ± 0.65	2.40 ± 0.55	2.00 ± 0.71	1.60 ± 0.89	0.163
4 weeks	2.60 ± 0.55*	2.00 ± 0.71	1.80 ± 0.45	1.40 ± 0.55	0.031
8 weeks	2.80 ± 0.45*,†	2.40 ± 0.55*,†	1.40 ± 0.55	0.80 ± 0.45	< 0.001

*: P < 0.05 vs. ABSP group; †: P < 0.05 vs. BSP group; #: P < 0.05 vs. PP group.

Immunohistochemical findings

The DNA content of a population of MSCs represented the number of MSCs on a scaffold, and was used as a measure of MSC proliferation on SIS meshes.

Microvessel density around the implants was quantified by counting CD31+ cells within the cluster of differentiation detected by immunohistochemistry at 1, 4, and 8 weeks (**Figure 7**). Microvessel densities were mostly lower in the model, PP, and BSP groups but higher in the ABSP group compared with normal rats at each time point (P < 0.05), with a significant difference between the model and normal groups at 4 weeks (P < 0.05). Microvessel density increased over time after operation, especially during the first 4 weeks. The differences between the ABSP and the remaining groups were statistically significant at 8 weeks (P < 0.01) (**Figure 7**).

As for COLI and III expression amounts, the normal group showed the highest values at each time point (1, 4, and 8 weeks post-implantation), followed by the ABSP group. Increases in COLI and III levels occurred over time, with significant differences observed in the PP and BSP groups relative to model rats (P < 0.05), which showed the lowest COLI and III expression levels (**Figures 8** and **9**). Meanwhile, COLI and III levels were higher in the ABSP group and lower in the PP group compared with the BSP group at all-time points; therefore, COLI and III levels in decreasing order were found in the normal, ABSP, BSP, PP, and model groups (**Figures 8** and **9**). These results indicated that

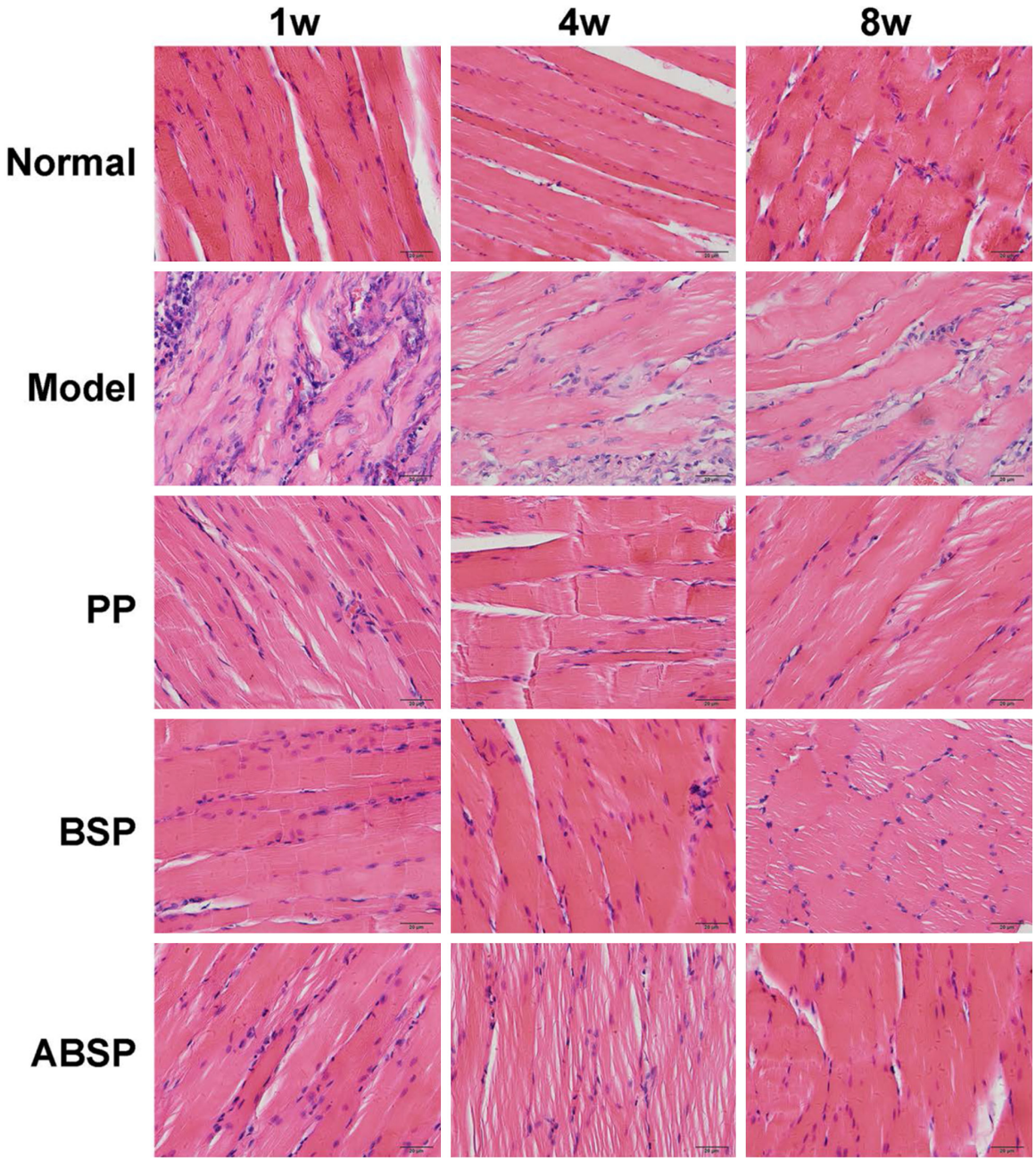

Figure 4. Histological examination of the tissue response to subcutaneously implanted meshes in a rat abdominal wall defect model at 1, 4, and 8 weeks after mesh implantation. Photomicrographs show SIS samples dyed with H&E. Normal abdominal tissue samples are presented in the top panels, followed by the Model, PP, BSP, and ABSP groups at 1, 4, and 8 weeks. Scale bar = 50 mm.

astragaloside IV-stimulated BMSCs seeded on SIS modified with PLGA NPs increased collagen production *in vivo*.

Expression of inflammatory and angiogenic factors

To determine whether the implanted mesh can repair abdominal wall defects, we analyzed the mRNA and protein levels of pro- and anti-inflammatory cytokines, ECM components, and angiogenic factors by qRT-PCR and WB, respectively, at 1, 4, and 8 weeks. MMP-9 and IL-6 mRNA levels declined in the ABSP group compared with other groups at each time point, except for the BSP group at 8 weeks (**Figure 10A**). On the other hand, the ABSP group showed a higher *COL1A1* mRNA level than the model and PP

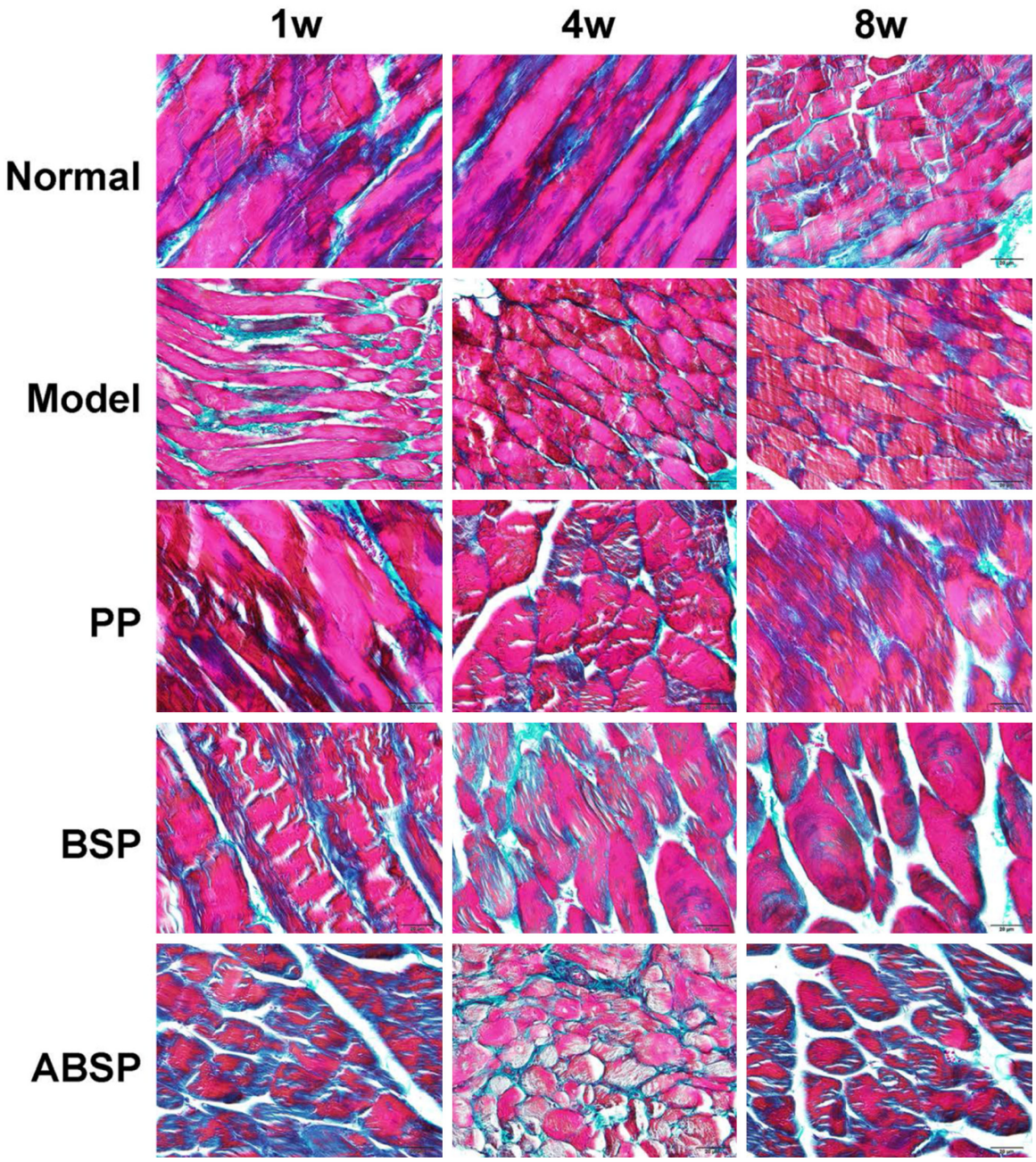

Figure 5. Masson's trichrome staining of abdominal wall tissue 1, 4, and 8 weeks after mesh implantation. Normal abdominal tissue samples are presented in the top panels, followed by the Model, PP, BSP, and ABSP groups at 1, 4, and 8 weeks. Scale bar = 50 mm. Collagen fibers and the muscle appear as blue and red, respectively.

groups at each time point ($P < 0.05$) and a slightly lower *COL1A1* mRNA level than the normal group at 4 and 8 weeks ($P > 0.05$). There were no differences in COL1A1 mRNA expression between the ABSP and BSP groups at any time point. COL3A1 mRNA expression showed a similar trend, although the level was lower in the ABSP compared with the normal group at 4 and 8 weeks. Angiogenesis is an important determinant of the survival of the implanted mesh; VEGF was upregulated in the ABSP group compared with the BSP, PP, and model groups, and downregulated relative to normal control values at 1, 4, and 8 weeks (**Figure 10A**). Similar trends in protein expression were found by WB (**Figure 10B**).

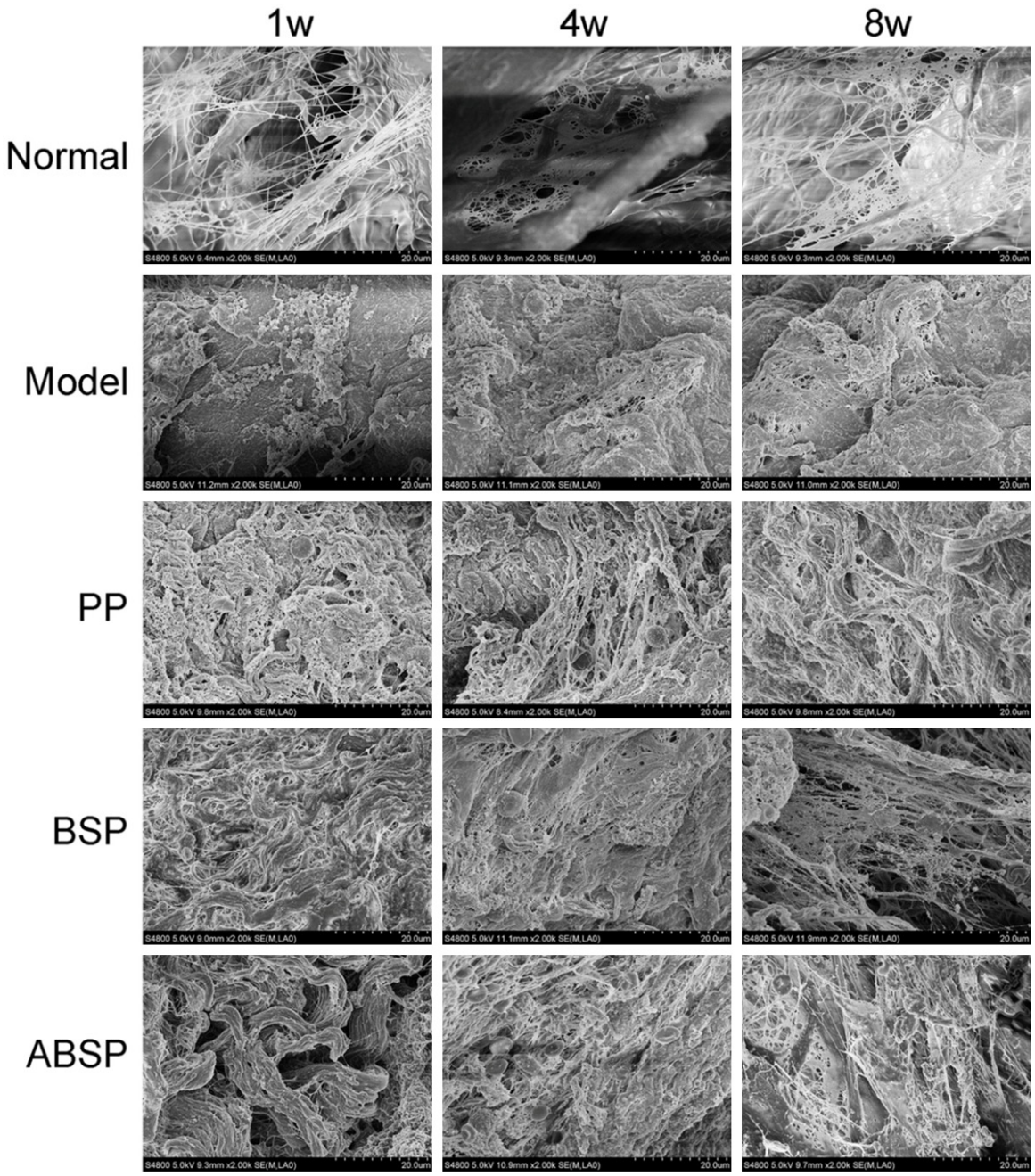

Figure 6. Ultrastructure of the abdominal wall tissue assessed by SEM at 1, 2, and 4 weeks after mesh implantation. Normal abdominal tissue samples are presented in the top panels, followed by the Model, PP, BSP, and ABSP groups at 1, 4, and 8 weeks. Scale bar = 20 μm.

Discussion

Our study designed a nano-biological mesh composed of aS-IV-induced BMSCs seeded on PLGA-NPs-SIS, which was demonstrated to be effective for abdominal wall reconstruction.

Reconstruction of abdominal wall defects with insufficient fascia musculares or excessive tension remains a clinical challenge. Besides operation, patches play an essential role in abdominal defect repair. The application of SIS to the engineering of manifold organs has yielded promising results in terms of host tissue regeneration and functional recovery [22]. To this end, various cell types have been used in conjunction with SIS [23]. As an acellular ECM, the SIS not only provides a three-dimensional

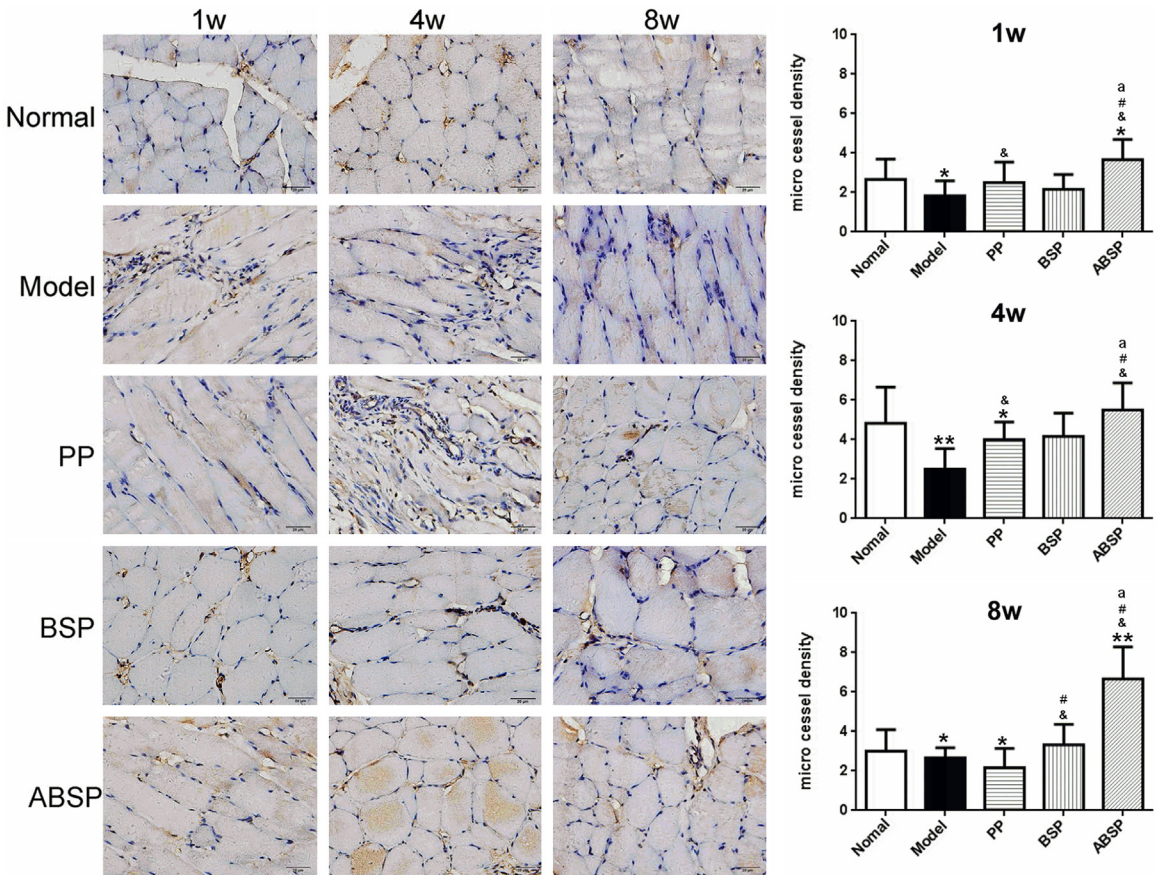

Figure 7. Immunohistochemical assessment of microvessel density in the abdominal wall tissue 1, 4, and 8 weeks after mesh implantation. By counting CD31 positive microvessels, microvessel density was assessed. Normal abdominal tissue samples are presented in the top image panels, followed by the Model, PP, BSP, and ABSP groups at 1, 4, and 8 weeks. Quantitation is shown in the right panels. *P < 0.05, **P < 0.01, vs. Normal group; &P < 0.05 vs. Model group; #P < 0.05 vs. PP group; aP < 0.05 vs. BSP group.

structure for cell adhesion, growth, and migration, but also secretes growth factors such as VEGF and glycosaminoglycan, fibronectin, laminin, heparin sulfate, COLIV, and hyaluronic acid [24, 25]. However, a previous study demonstrated that although it promoted cell attachment, proliferation, and differentiation, SIS only induced partial epithelialization 35 days after esophagoplasty [26].

SIS can support BMSCs without affecting cell viability, with collagen, elastin, as well as collagen crosslinking stored in culture [27]. BMSCs are critical for the repair of damaged tissue since they release various growth factors and cytokines [28]. Implanted BMSCs loaded on SIS have been successfully engrafted and differentiated into myocyte-like cells at the site of implantation, accelerating re-epithelialization, revascularization, and muscular regeneration to a greater extent than SIS only [12]. aS-IV was extracted from *Astragalus membranaceus*, and is usually used as a food additive and in herbal medicine for positively inotropic features as well as anti-hypertensive, -inflammatory, -oxidant, and -infarction properties [29]. aS-IV was shown to upregulate VEGF and inhibit leukocyte infiltration and the expression of inflammatory factors including TNF-α and IL-1β and -6 [30]. In our study, aS-IV in the 0-160 μg/ml range inhibited BMSC proliferation in a concentration-dependent manner (**Figure 2**). Then, in vivo experiments showed that collagen was upregulated by SIS loaded with BMSCs stimulated with aS-IV (**Figure 5**), which was confirmed by SEM (**Figure 6**) and immunohistochemistry (**Figures 8** and **9**).

A key factor in abdominal wall reconstruction with a biological mesh is the balance between

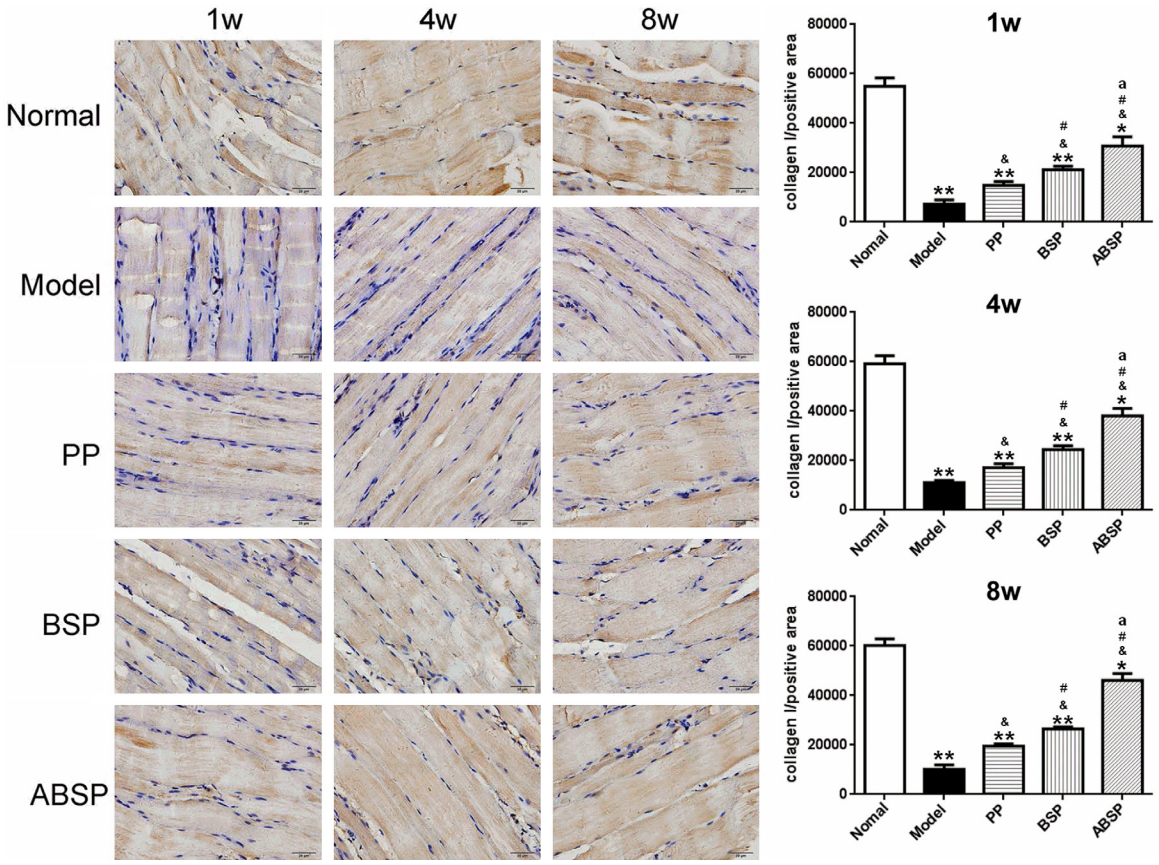

Figure 8. Immunohistochemical assessment of COLI protein amounts in the abdominal wall tissue 1, 4, and 8 weeks after mesh implantation. Normal abdominal tissue samples are presented in the top image panels, followed by the Model, PP, BSP, and ABSP groups at 1, 4, and 8 weeks. Quantitation is shown in the right panels. *P < 0.05, **P < 0.01, vs. Normal group; &P < 0.05 vs. Model group; #P < 0.05 vs. PP group; aP < 0.05 vs. BSP group.

rates of mesh degradation and tissue remodeling. If the mesh has sufficient mechanical strength to prevent herniation before complete degradation, the probability of hernia recurrence is significantly lowered. In a canine model of abdominal wall defect repair, 25% of SIS scaffolds were absorbed after 1 month and 75% after 2 months; after 4 months, the scaffold was completely replaced with host tissue [31]. Cell-SIS scaffolds are more effective in minimizing the incidence of hernia than those consisting of SIS alone [5]. In this study, BMSCs stimulated by aS-IV and seeded on a SIS-PLGA scaffold produced COLI and COLIII (**Figure 3**), and SEM revealed that the scaffold was eventually covered by fibrous connective tissue and mesothelial cells. In agreement, qRT-PCR and WB revealed that *COLIII* mRNA expression increased in the BSP and ABSP groups compared with the PP group, although COLIII protein levels were similar in the two former groups. It is known that collagen is a biomarker of osteogenesis, and the up-regulated COLI and COLIII in BMSCs are helpful to promote osteogenesis and play the role of abdominal wall reconstruction [32].

Capillaries supply oxygen and nutrients to engineered or regenerated tissue that prevents cell necrosis. A combination of BMSCs and SIS was found to synergistically induce angiogenesis in a rat esophageal defect model, with neovascularization improving blood supply to the defect and enhancing tissue repair. Indeed, engrafted BMSCs can produce angiogenic and stem cell homing factors via a paracrine mechanism critical for angiogenesis [24]. In this study, we observed neovascularization and increased microvessel density in the BSP and ABSP groups, as demonstrated by elevated amounts of CD31+ cells (**Figure 7**); thus, aS-IV stimulation of BMSCs seeded on SIS-PLGA scaffolds may enhance neovascularization,

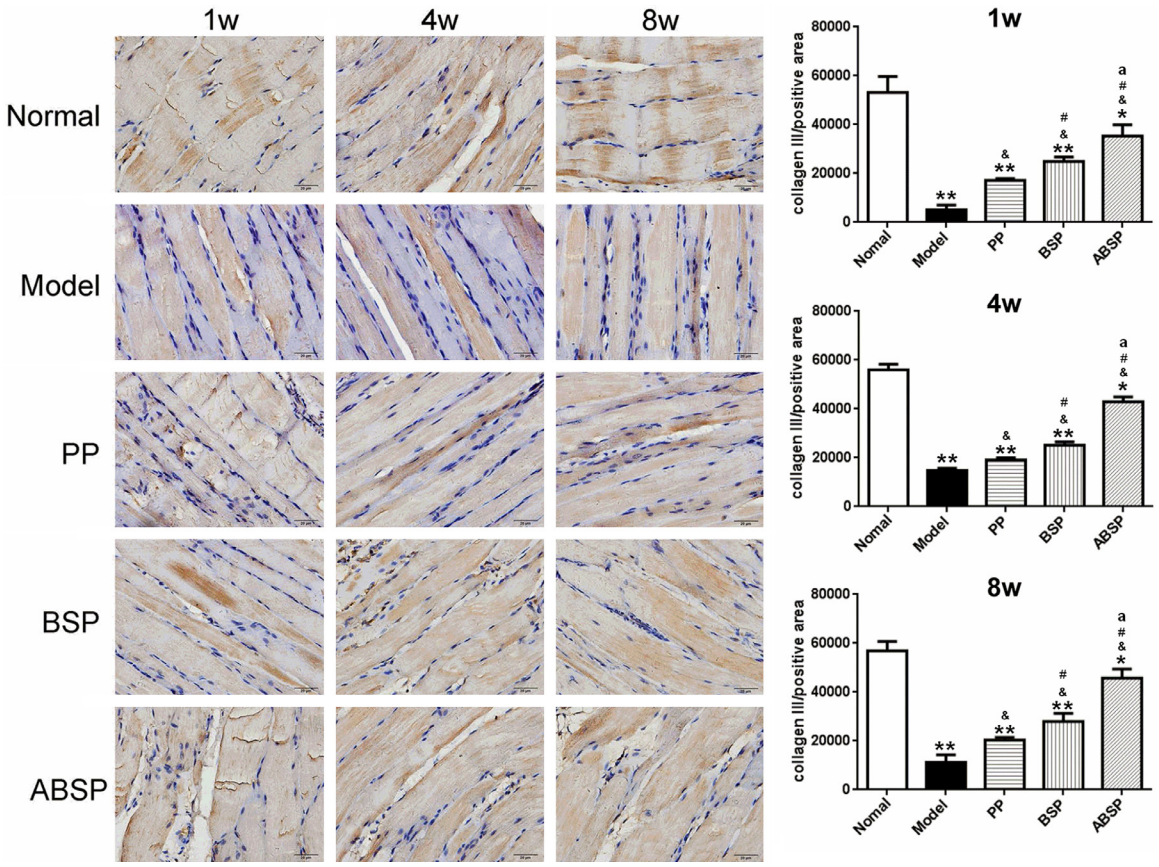

Figure 9. Immunohistochemical assessment of COLIII protein amounts in the abdominal wall tissue 1, 4, and 8 weeks after mesh implantation. Normal abdominal tissue samples are presented in the top image panels, followed by the Model, PP, BSP, and ABSP groups at 1, 4, and 8 weeks. Quantitation is shown in the right panels. *P < 0.05, **P < 0.01, vs. Normal group; &P < 0.05 vs. Model group; #P < 0.05 vs. PP group; aP < 0.05 vs. BSP group.

which can, in turn, promote cell infiltration. CD31 staining data were comparable across groups in our study, implying that MSC seeding failed to change the ability of SIS to integrate into the surrounding myocardium or recruit new blood vessels.

It is likely that the non-injury model established here may have provided insufficient stimulus for the pro-regenerative activity of BMSCs.

Mesh implantation results in a more persistent inflammatory reaction than SIS implantation, as demonstrated by elevated amounts of mast cells, CD8+ T cells, as well as CD68+ macrophages 24 weeks after surgery [33]. The existence of MSCs can suppress graft-specific adaptive immune responses compared with SIS alone. As shown above, macroscopic examination revealed that the ABSP group had reduced inflammatory response compared with the model, PP, and BSP groups, which may be associated with reduced adhesion of abdominal organs such as the intestines, liver margin, and omentum that can cause intestinal obstruction, abdominal organ failure, and peritonitis. Secretion of cytokines (IL-6) and ECM components (MMP-9) by BMSCs was reduced after cell activation by aS-IV, although the level differences were insignificant. It can be attributed to the suppression of the inflammatory response in the ABSP group compared with the BSP and PP groups. These findings suggest a potential therapeutic benefit for aS-IV-induced BMSCs seeded on SIS through increased release of pro-angiogenic cytokines.

The ideal biosynthetic material should not be altered by tissue fluid. It is a chemically inert material that does not induce inflammation and is also a non-carcinogenic material that can resist mechanical stress, does not cause allergic reaction or anaphylaxis, and can be molded

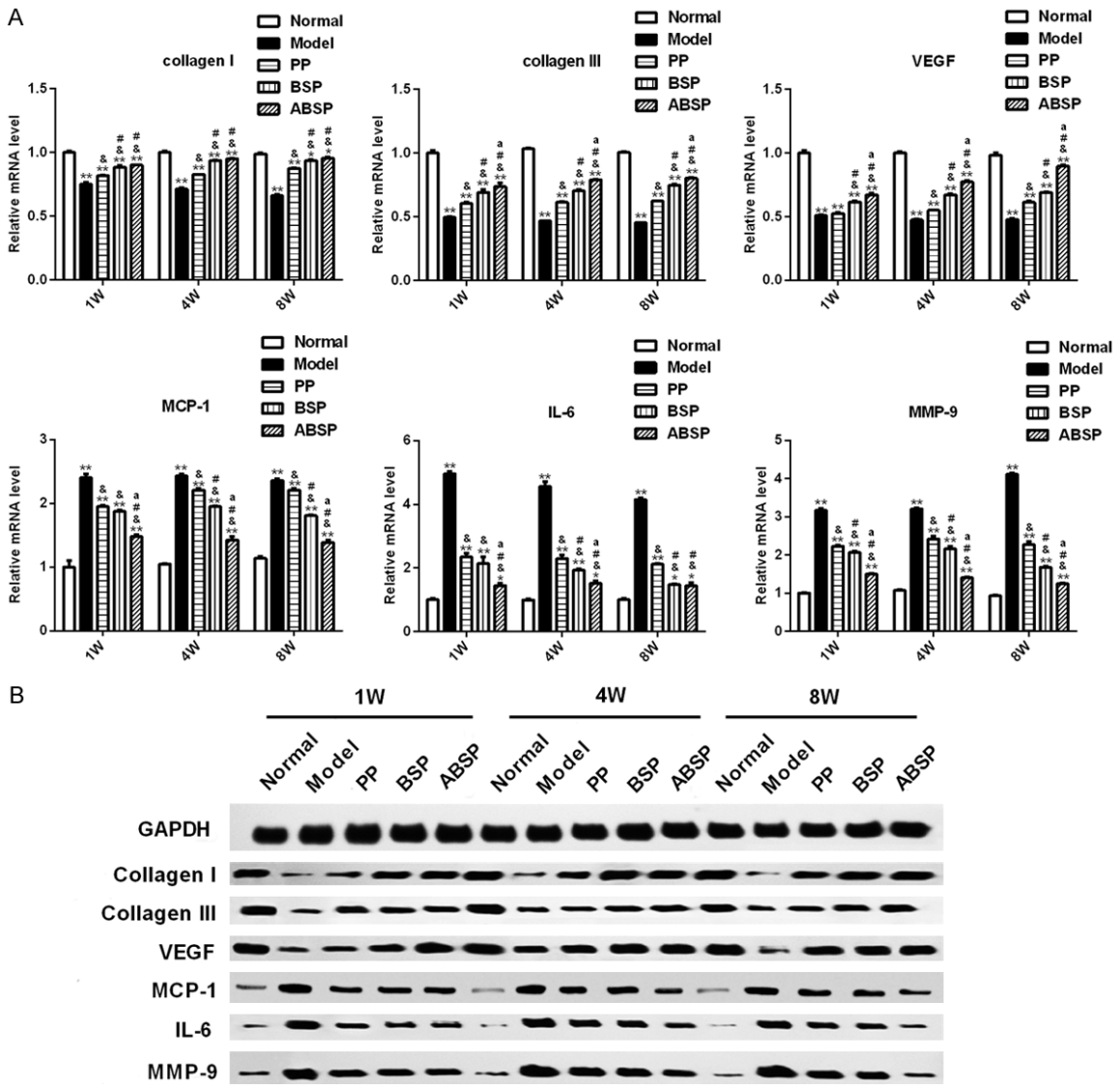

Figure 10. Protein and mRNA expression of inflammatory and angiogenic factors. A. qRT-PCR analysis of COL1A1, COL3A1, VEGF, MMP-9, MCP-1, and IL-6 levels; relative mRNA levels are based on GAPDH expression. B. WB analysis of the expression of indicated proteins (GAPDH was adopted as a loading control). *P < 0.05, **P < 0.01, vs. Normal group; &P < 0.05 vs. Model group; #P < 0.05 vs. PP group; aP < 0.05 vs. BSP group.

into different shapes as needed. In our study, we analyzed the feasibility of using a mesh consisting of BMSCs seeded on SIS modified with PLGA NPs for abdominal wall defect repair in a rat model. Compared with the PP mesh, this graft showed a higher capacity for autologous muscle regeneration and remodeling of the nearby tissues while suppressing the inflammatory response. These findings underscore the importance of naturally occurring products in designing complex tools to solve actual clinical problems. It is worth assessing additional compounds with properties similar to those of aS-IV in order to identify the best inducers of BMSCs, which would yield even better platforms for abdominal wall reconstruction.

The main limitation of this study is the use of rats, which lacks the abdominal aponeurosis-like tissue found in humans and cannot mimic the process of normal musculofascial tissue defect repair. Therefore, our findings should be confirmed in clinical trials before application of this platform.

In conclusion, the nano-biological mesh composed of a S-IV-induced BMSCs seeded on

PLGA-NPs-SIS can be used for abdominal wall reconstruction. Therefore, the engineered biomaterial has the potential for tissue engineering in clinical applications.

Acknowledgements

This work was supported by grants from China National Science Funds (grant no. 81202821), Zhejiang Provincial Natural Science Foundation of China (grant no. 2103KYA169), and Hangzhou Municipal Science and Technology Commission fund (grant no. 20170533B87). This study is financially supported by National Natural Science Foundation of China Youth Science Foundation (grant no. 81202821), Zhejiang Medical and Health Science and Technology Program (grant no. 2013KYA169).

Disclosure of conflict of interest

None.

Address correspondence to: Hai Huang, Department of General Surgery, Guangxing Affiliated Hospital of Zhejiang Chinese Medical University, No.453 Stadium Road, Hangzhou 310007, Zhejiang Provincial, China. Tel: +86-0571-88950832; E-mail: haihuang1593@outlook.com

References

[1] Skrobot J, Zair L, Ostrowski M and El Fray M. New injectable elastomeric biomaterials for hernia repair and their biocompatibility. Biomaterials 2016; 75: 182-192.

[2] Johnson KC, Miller MT, Plymale MA, Levy S, Davenport DL and Roth JS. Abdominal wall reconstruction: a comparison of totally extraperitoneal and transabdominal preperitoneal approaches. J Am Coll Surg 2016; 222: 159-165.

[3] Diaz-Siso JR, Bueno EM and Pomahac B. Abdominal wall reconstruction using a non-cross-linked porcine dermal scaffold: a follow-up study. Hernia 2013; 17: 37-44.

[4] Sosin M, Patel KM, Albino FP, Nahabedian MY and Bhanot P. A patient-centered appraisal of outcomes following abdominal wall reconstruction: a systematic review of the current literature. Plast Reconstr Surg 2014; 133: 408-418.

[5] Song Z, Peng Z, Liu Z, Yang J, Tang R and Gu Y. Reconstruction of abdominal wall musculofascial defects with small intestinal submucosa scaffolds seeded with tenocytes in rats. Tissue Eng Part A 2013; 19: 1543-1553.

[6] Klinger A, Kawata M, Villalobos M, Jones RB, Pike S, Wu N, Chang S, Zhang P, DiMuzio P, Vernengo J, Benvenuto P, Goldfarb RD, Hunter K, Liu Y, Carpenter JP and Tulenko TN. Living scaffolds: surgical repair using scaffolds seeded with human adipose-derived stem cells. Hernia 2016; 20: 161-170.

[7] Franklin M and Russek K. Use of porcine small intestine submucosa as a prosthetic material for laparoscopic hernia repair in infected and potentially contaminated fields: long-term follow-up assessment. Surg Endosc 2011; 25: 1693-1694.

[8] Rauth TP, Poulose BK, Nanney LB and Holzman MD. A comparative analysis of expanded polytetrafluoroethylene and small intestinal submucosa-implications for patch repair in ventral herniorrhaphy. J Surg Res 2007; 143: 43-49.

[9] Madani A, Niculiseanu P, Marini W, Kaneva PA, Mappin-Kasirer B, Vassiliou MC, Khwaja K, Fata P, Fried GM and Feldman LS. Biologic mesh for repair of ventral hernias in contaminated fields: long-term clinical and patient-reported outcomes. Surg Endosc 2017; 31: 861-871.

[10] Wu W, Li B, Liu Y, Wang X and Tang L. Effect of multilaminate small intestinal submucosa as a barrier membrane on bone formation in a rabbit mandible defect model. Biomed Res Int 2018; 2018: 3270293.

[11] FitzGerald JF and Kumar AS. Biologic versus Synthetic mesh reinforcement: what are the pros and cons? Clin Colon Rectal Surg 2014; 27: 140-148.

[12] Tan B, Wei RQ, Tan MY, Luo JC, Deng L, Chen XH, Hou JL, Li XQ, Yang ZM and Xie HQ. Tissue engineered esophagus by mesenchymal stem cell seeding for esophageal repair in a canine model. J Surg Res 2013; 182: 40-48.

[13] Zhang Y, Lin HK, Frimberger D, Epstein RB and Kropp BP. Growth of bone marrow stromal cells on small intestinal submucosa: an alternative cell source for tissue engineered bladder. BJU Int 2005; 96: 1120-1125.

[14] Jia L, Lv D, Zhang S, Wang Z and Zhou B. Astragaloside IV inhibits the progression of non-small cell lung cancer through the Akt/GSK-3beta/beta-catenin pathway. Oncol Res 2019; 27: 503-508.

[15] Xie J, Wang H, Song T, Wang Z, Li F, Ma J, Chen J, Nan Y, Yi H and Wang W. Tanshinone IIA and astragaloside IV promote the migration of mesenchymal stem cells by up-regulation of CXCR4. Protoplasma 2013; 250: 521-530.

[16] Che X, Wang Q, Xie Y, Xu W, Shao X, Mou S and Ni Z. Astragaloside IV suppresses transforming growth factor-beta1 induced fibrosis of cultured mouse renal fibroblasts via inhibition of the MAPK and NF-kappaB signaling pathways. Biochem Biophys Res Commun 2015; 464: 1260-1266.

[17] Tahara K, Samura S, Tsuji K, Yamamoto H, Tsukada Y, Bando Y, Tsujimoto H, Morishita R and Kawashima Y. Oral nuclear factor-kappaB decoy oligonucleotides delivery system with chitosan modified poly (D,L-lactide-co-glycolide) nanospheres for inflammatory bowel disease. Biomaterials 2011; 32: 870-878.

[18] Yu Z, Zhu T, Li C, Shi X, Liu X, Yang X and Sun H. Improvement of intertrochanteric bone quality in osteoporotic female rats after injection of polylactic acid-polyglycolic acid copolymer/collagen type I microspheres combined with bone mesenchymal stem cells. Int Orthop 2012; 36: 2163-2171.

[19] Pang X, Pan Y, Hua F, Sun C, Chen L, Chen F, Zhu K, Xu J and Chen M. Effects of PLGA absorbable membrane on preventing postoperative abdominal adhesion in rabbits. Zhongguo Yi Liao Qi Xie Za Zhi 2014; 38: 389-392.

[20] Schnoor B, Elhendawy A, Joseph S, Putman M, Chacon-Cerdas R, Flores-Mora D, Bravo-Moraga F, Gonzalez-Nilo F and Salvador-Morales C. Engineering atrazine loaded poly (lactic- coglycolic acid) nanoparticles to ameliorate environmental challenges. J Agric Food Chem 2018; 66: 7889-7898.

[21] Raghavan D, Kropp BP, Lin HK, Zhang Y, Cowan R and Madihally SV. Physical characteristics of small intestinal submucosa scaffolds are location-dependent. J Biomed Mater Res A 2005; 73: 90-96.

[22] Badylak SF. The extracellular matrix as a biologic scaffold material. Biomaterials 2007; 28: 3587-3593.

[23] Conconi MT, De Coppi P, Bellini S, Zara G, Sabatti M, Marzaro M, Zanon GF, Gamba PG, Parnigotto PP and Nussdorfer GG. Homologous muscle acellular matrix seeded with autologous myoblasts as a tissue-engineering approach to abdominal wall-defect repair. Biomaterials 2005; 26: 2567-2574.

[24] Kim K and Kim MS. An injectable hydrogel derived from small intestine submucosa as a stem cell carrier. J Biomed Mater Res B Appl Biomater 2016; 104: 1544-1550.

[25] Luo JC, Chen W, Chen XH, Qin TW, Huang YC, Xie HQ, Li XQ, Qian ZY and Yang ZM. A multi-step method for preparation of porcine small intestinal submucosa (SIS). Biomaterials 2011; 32: 706-713.

[26] Badylak S, Meurling S, Chen M, Spievack A and Simmons-Byrd A. Resorbable bioscaffold for esophageal repair in a dog model. J Pediatr Surg 2000; 35: 1097-1103.

[27] Wang D, Ding X, Xue W, Zheng J, Tian X, Li Y, Wang X, Song H, Liu H and Luo X. A new scaffold containing small intestinal submucosa and mesenchymal stem cells improves pancreatic islet function and survival in vitro and in vivo. Int J Mol Med 2017; 39: 167-173.

[28] McFarlin K, Gao X, Liu YB, Dulchavsky DS, Kwon D, Arbab AS, Bansal M, Li Y, Chopp M, Dulchavsky SA and Gautam SC. Bone marrow-derived mesenchymal stromal cells accelerate wound healing in the rat. Wound Repair Regen 2006; 14: 471-478.

[29] Liu X, Zhang J, Wang S, Qiu J and Yu C. Astragaloside IV attenuates the H2O2-induced apoptosis of neuronal cells by inhibiting alpha-synuclein expression via the p38 MAPK pathway. Int J Mol Med 2017; 40: 1772-1780.

[30] Lin R, Chen H, Callow D, Li S, Wang L, Li S, Chen L, Ding J, Gao W, Xu H, Kong J and Zhou K. Multifaceted effects of astragaloside IV on promotion of random pattern skin flap survival in rats. Am J Transl Res 2017; 9: 4161-4172.

[31] Clarke KM, Lantz GC, Salisbury SK, Badylak SF, Hiles MC and Voytik SL. Intestine submucosa and polypropylene mesh for abdominal wall repair in dogs. J Surg Res 1996; 60: 107-114.

[32] Elango J, Robinson J, Zhang J, Bao B, Ma N, de Val J and Wu W. Collagen peptide upregulates osteoblastogenesis from bone marrow mesenchymal stem cells through MAPK-Runx2. Cells 2019; 8: 446.

[33] Lee AJ, Lee SH, Chung WH, Kim DH, Chung DJ, Do SH and Kim HY. Evaluation of a canine small intestinal submucosal xenograft and polypropylene mesh as bioscaffolds in an abdominal full-thickness resection model of growing rats. J Vet Sci 2013; 14: 175-184.